HHS Public Access

Author manuscript

Biosens Bioelectron. Author manuscript; available in PMC 2019 November 15.

Published in final edited form as:

Biosens Bioelectron. 2018 November 15; 119: 221–229. doi:10.1016/j.bios.2018.07.062.

In Situ, Amplification-Free Double-Stranded Mutation Detection at 60 copies/ml with thousand-fold Wild Type in Urine

Ceyhun Kirimli[a], **Selena Lin**[b], **Ying-His Su**[c,d], **Wei-Heng Shih**[e], and **Wan Y. Shih**[f]

[a]School of Biomedical Engineering, Science, and Health System, Drexel University, Philadelphia, PA 19104

[b]Department of Microbiology and Immunology, Drexel University College of Medicine, Philadelphia, PA, 19104

[c]The Baruch S. Blumberg Institute, Doylestown, PA 18901

[d]Department of Immunology and Microbiology, Drexel University

[e]Department of Materials Science and Engineering, Drexel University, Philadelphia, PA 19104

[f]School of Biomedical Engineering, Science, and Health System, Drexel University, Philadelphia, PA 19104

Abstract

We have investigated amplification-free *in situ* double-stranded mutation detection in urine in the concentration range 10^{-19}M – 10^{-16} M using piezoelectric plate sensors (PEPs). The detection was carried out in a close-loop flow with two temperature zones. The 95°C high-temperature zone served as the reservoir where the sample was loaded and DNA de-hybridized. The heated urine was cooled flowing through a 1 m long tubing immersed in room-temperature water bath at a flow rate of 4 ml/min to reach the detection cell at the desire detection temperature for the detection to take place. With hepatitis B virus double mutation (HBVDM) and KRAS G12V point mutation as model double mutations, it is shown that PEPS was able to detect double-stranded HBVDM and KRAS with 70% detection efficiency or better at concentration as low as 10^{-19}M against single-stranded mutation detection at the same concentrations, which was validated by the following *in situ* fluorescent reporter microspheres (FRMs) detection as well as microscopic visualization of the FRMs bound to the captured mutant on the PEPS surface. Furthermore, the same double-stranded mutation detection efficacy was demonstrated at 10^{-19} M – 10^{-16} M in a background of 250-fold wildtype for HBVDM and 1000-fold wildtype for KRAS. Also demonstrated was detection of KRAS mutation at 10^{-19} M – 10^{-16} M of SW480 DNA fragments in urine.

Keywords

label-free mutation detection; amplification-free mutation detection; isolation-free mutation detection; label-free double-stranded DNA detection; high-specificity mutation detection

I. INTRODUCTION

Detecting gene mutation is essential for cancer diagnosis, and therapy decision and efficacy monitoring. Traditionally mutation detection is done by gene sequencing which requires solid tumor samples and is expensive. Additionally, making therapeutic decisions based on the gene sequencing results from a single biopsy can be difficult due to tumor heterogeneity[1]. Biopsy procedures for internal organs are also intrusive and not performed in some cases due to the increased risk of tumor seeding to other sites[2]. This makes body fluids such as blood or urine highly desirable as the source for cancer genetic marker detection. Polymerase chain reaction (PCR) has been the most investigated methods for detecting circulating genetic markers in which PCR is followed by melting temperature analysis to differentiate mutant (MT) from the wild type (WT), the normal form of the gene. So far, detecting mutations in sera or urine using PCR has been challenging due to the fact that the melting-temperature difference between a single-nucleotide MT and the WT can be only a few degrees[3], the concentration of circulating MT are extremely low ($<10^{-18}$ M or 600 copies/ml)[4], MT is outnumbered by the WT by > 240 times[5]. In urine, trans-renal deoxyribonucleic acid (DNA) exist in the form of short fragments often less than 200 base pairs (bp),[6] which further decreases the sensitivity of PCR because only a small fraction of the naturally occurring fragments in urine can be amplified.[5, 7]

Genetic detection technologies currently under development rely on fluorescence[8], quartz crystal microbalance (QCM)[9, 10], electrochemistry[11], binding to nano-metal particles[12], surface plasmon resonance (SPR)[13], silicon-based microcantilever sensor as well as piezoelectric microcantilever sensor. For DNA detection, nanoparticle-amplified QCM exhibited a concentration sensitivity of 1 pM[14]. Nanoparticle-enhanced SPR exhibited concentration sensitivity of 10–100 aM[15]. The electrochemical methods involving nanofibers and nanotubes exhibited concentration sensitivity of about 30 fM[16]. Nanowires[17–21], and nanotubes[22, 23] exhibited concentration sensitivity ranging 1–100 fM. Microcantilevers coupled with nano-metal particles exhibited 0.01 nM sensitivity[24]. Although methods such as QCM, SPR, silicon-based microcantilever sensor as well as lead zirconate titanate (PZT) piezoelectric microcantilever sensor (PEMS)[25, 26] are label-free, the sensitivity was still many orders of magnitude away from the attomolar (aM, or 10^{-18}M) requirement. Similarly, the 10^{-16} M sensitivity achieved by magnetic beads isolation coupled with electrochemical enhancement was still not sufficient[27]. Nano-scale mechanical imaging by atomic force microscopy (AFM) could differentiate unhybridized single-stranded DNAs (ssDNAs) from hybridized double-stranded DNAs (dsDNAs) at aM sensitivity but it required sophisticated instrument such as AFM[28]. Carbon nanotube impedance biosensors exhibited 100 aM sensitivity in DNA detection, which was insufficient for clinical applications[29]. GaN nanowire extended-gate field-effect-transistors[30] and streptavidin horseradish peroxidase functionalized carbon nanotubes[31] have aM sensitivity in DNA detection. However, these detections are not *in situ* they typically require washing steps before the measurements can be made. Peptide nucleic acid (PNA) probe-enhanced electrochemical biosensors based on an integrated chip also exhibited aM sensitivity. However, they also required washing[32]. Recently a disposable electrochemical biosensor based on magnetic bead amplification and target DNA biotinylation exhibited aM

sensitivity[33]. However, it required multiple steps of amplification and the need to biotinylate the target DNA rendering it impractical[33]. Note most of these methods detected only single-stranded DNAs and did not address how to detect double-stranded DNAs while DNAs are naturally double-stranded.

A lead magnesium niobate–lead titanate $(Pb(Mg_{1/3}Nb_{2/3})O_3)_{0.65}(PbTiO_3)_{0.35}$ (PMN-PT) piezoelectric plate sensor (PEPS) is a unique sensor consisting of a PMN-PT freestanding film 8 μm in thickness[34] coated with gold electrodes on the two major surfaces and encapsulated with a thin electrical insulation layer. By covalently immobilizing a probe DNA (probe) complementary to a target DNA (tDNA) and immersing the probe-coated PEPS in a biological fluid sample, binding of the tDNA from the biological fluid sample to the probe on PEPS surface shifts the PEPS length extension mode (LEM) or the width extension mode (WEM) resonance frequency, f. *In situ* detection of the tDNA from the biological fluid sample has been achieved by monitoring the PEPS LEM [35] or WEM[36] resonance frequency shift, Δf, in real time. What is unique about PEPS is its ability to enhance the detection Δf more than 1000-fold than by mass change alone due to the crystalline orientation change in the PMN-PT layer induced by the binding of the target analyte to the receptor on the PEPS surface[35, 37–41]. As a result, PEPS has been demonstrated capable of detecting single-stranded DNA with PCR-like sensitivity (10^{-19}M) without the need of amplification in urine. With temperature control and a flow, it was further demonstrated that not only could a PEPS achieve 10^{-19} M sensitivity without amplification but do so with a high background of the wildtype (WT). For example, hepatitis B virus (BHV) 1762T/1764A double mutation (HBVDM) detection in urine was done with 250-fold WT[42] while KRAS (G12V) point mutation (PM) detection in urine was done with 1000-fold WT[43]. Although such high sensitivity and specificity is highly desirable for potential circulating mutation detection the drawback is that these results were based on single-stranded DNA detection whereas in patient samples the DNAs are naturally double stranded. In order for PEPS mutation detection to be truly isolation-free and amplification-free it must be able to detect double-stranded mutations *in situ*.

The goal of this study is to further investigate the feasibility of *in situ* sensitively and specifically detecting double-stranded mutations in urine with a high background of WT using a PMN-PT PEPS. To do so, we would utilize a flow system with two temperature zones. The high-temperature zone dubbed “the reservoir” was where the sample was loaded and the DNA dehybridized. The lower-temperature zone dubbed “the detection cell” was kept at the detection temperature so that specific mutation detection by the PEPS could take place. HBVDM and KRAS G12V PM were chosen as the model double-stranded mutations for ease of comparison with detection of their single-stranded counterparts as both mutations have been extensively studied in single-stranded mutation detections.

II. EXPERIMENTAL

II.1. Probe, MT, WT, and reporter DNAs (rDNAs)

The probe for HBVDM MT was 16-nt long containing the sense sequence complementary to the targeted antisense strand of the HBVDM MT (GeneBank Accession #X04615) centered at the 1762T/1764A mutation site. The probe for KRAS G12V MT was 17-nt long

containing the sense sequence complementary to the targeted antisense strand of the KRAS G12V mutation (Gene ID:3845) centered at the mutation site.[42, 44] The KRAS probe also contained three consecutive locked nucleic acid (LNA) bases centered about the mutation site. Both probes were amine-activated with a 12-polyethyleneglycol (PEG) spacer at the 5' end. The 90-nt targeted antisense strand of the double-stranded HBVDM and KRAS (Sigma) along with the sequences of their probes are shown in Table I. Note that the probes are perfectly complementary to the MT but not the WT--The HBVDM probe had two mismatches with the HBVDM WT while the KRAS probe had one mismatch with the KRAS WT. As such, the melting temperatures for the probe to the WT were lower than those of the probe to the MT (see Table I) to permit the probe to specifically bind only to MT but not WT at a temperature lower than the melting temperature of the probe-to-MT bonding but higher than that of the probe-to-WT bonding. In Table I in the supplemental information we also show the sequences of the reporter DNAs (rDNAs). The rDNAs were amine-activated sense sequences complementary to the antisense sequences of the target DNA immediately upstream and downstream the sequence targeted by the probe. The rDNAs would be covalently bound to the fluorescent reporter microspheres (FRMs) as described below for validation of the tDNA detection. In Figs. 1a and 1b schematics are shown to illustrate the hybridisation schemes of the probe to the MT and WT as well as that for the rDNAs to the MT and WT for HBVDM and KRAS G12V, respectively.

II.2. Fluorescent reporter microspheres (FRMs)

Carboxylated fluorescent microspheres 6 μm in diameter emitting blue light (Bright Blue (BB) (≈Coumarin), Polysciences) were used as FRMs to report binding of the target DNA to the probe on the PEPS surface. To covalently bond the rDNAs to the FRMs, the carboxyl groups on the FRMs were reacted to the amine end of both the upstream and downstream rDNAs in 1:1 ratio in the presence of 5 mg ml^{-1} of 1-ethyl-3-(3-dimethylaminopropyl)carbodiimide (EDC) (Pierce) and 5 mg ml^{-1} of N-hydroxysulfosuccinimide (sulfo-NHS) (Pierce) at pH = 7 for 1 hr as described before.[35, 36, 42, 44–46] Once the rDNAs were covalently bound on the surface, FRMs could be used for both *in situ* detection validation as well as microscopic visual validation as described before. For *in situ* detection validation, the total volume of the FRMs suspension was 8 ml with a concentration 1×10^5 FRMs ml^{-1}. At a flow rate of 2 ml min^{-1}, the 8 ml of the FRMs suspension was cycled approximately 7 times during the 30 minutes of the FRM detection step.

II.3. SW480 DNA Fragments

In addition to detecting double-stranded synthetic KRAS G12V, detection of human KRAS G12V point mutation in urine was carried out by spiking SW480 DNA fragments in urine. SW480 (ATCC) is a human cell line homozygous for the KRAS G12V point mutation. SW480 DNA were extracted from SW480 cell culture using a DNA isolation kit (Qiagen DNeasy Blood & Tissue Kit) and sonicated to produce SW480 DNA fragments of about 200–400 base pairs (bp) to mimic DNA fragments in urine. The DNA concentration was determined by spectrophotometry using NanoDrop Spectrophotometer (Thermo Fisher Scientific, Waltham, MA, USA) and then confirmed by a quantitative PCR assay for beta-

globin gene using the LightCycler® Control Kit DNA (Roche Diagnostics Corporation, Indianapolis, IN, USA)

II.4. PEPS fabrication

Details of the PEPS fabrication procedure can be found in previous publications[36, 42, 43]. An optical micrograph of the top-view of a PEPS used in this study made from PMN-PT freestanding films 8 μm in thickness coated with a 110 nm thick Cr/Au electrode by thermal evaporation (Thermionics VE 90) is shown in the insert of Fig. 2a.

II.5. Electrical Insulation and PEPS in liquid Stability

The PEPS was electrically insulated for in-liquid stability using a continuous 3-mercaptopropyltrimethoxysilane (MPS) (Sigma) solution coating method.[47] The in-liquid stability of the PEPS was achieved by continuously coating the PEPS with 3-mercaptopropyltrimethoxysilane (MPS) as described previously followed by a resonance peak frequency stability test. A PEPS would not be used for detection until its width-extension-mode (WEM) resonance frequency in phosphate buffer saline (PBS) solution (~3MHz) achieved a standard deviation of < 20 Hz in 30 min.

II.6. Probe Immobilization

The MPS insulation also served as the anchor to immobilize the probe via a bifunctional linker sulfosuccinimidyl-4-(N-maleimidomethyl)cyclohexane-1-carboxylate (sulfo-SMCC) (Pierce). The MPS-coated PEPS was first immersed in 200 μL of a 5 mM sulfo-SMCC solution in phosphate buffer saline (PBS) solution for 1 hour to immobilize sulfo-SMCC on the PEPS surface by reacting the maleimide of the sulfo-SMCC to the thiol of the MPS followed by washing three times with deionized (DI) water. The sulfo-SMCC-reacted PEPS was then immersed in 200 μL of 10 μM of amine-activated probe solution in PBS for 30 min followed by washing in DI water for three times. Note that the pKa of thiol was about 10.5. As such it was expected that most of the thiols would be un-oxidized and could readily react with the maleimide of the sulfo-SMCC under the pH of PBS during immobilization, which was about 7. Indeed, the probe immobilized on the MPS surface was quantified using a quartz crystal microbalance (QCM) to be about 3–4 probes per 100 nm^2.[48] This indicates that the SH of the MPS was indeed effective to facilitate the immobilization of the probe.

II.7. Nonspecific Binding Blocking

After probe immobilization, the PEPS was treated with 3% bovine serum albumin (Sigma) in PBS for 1 h followed by washing 5 times with PBS. As demonstrated by the previous study, 3% BSA was sufficient to completely block the nonspecific bindings for DNA detection in urine.[36]

II.8. Resonance Frequency Monitoring

Electrical impedance spectra were measured to monitor the resonance spectra of a PEPS using a portable AIM 4170C impedance analyzer (Array Solutions). Typical in-air and in-PBS phase angle-versus-frequency resonance spectra of the PEPS shown in the insert of Fig. 2a are shown in Fig. 2a. As can be seen, the base-line, the length-extension mode (LEM)

resonance peak, and the width-extension-mode resonance (WEM) peak of the in-liquid spectrum were close to those of the in-air spectrum, indicating the effectiveness of the MPS insulation coating. In all the following experiments, the WEM peak of the resonance spectrum was monitored for detection. In Fig. 2b we plot the resonance frequency shift versus time during the various steps of PEPS preparation and detection for illustration purposes. As can be seen the relative resonance frequency shift, Δf/f, of the first WEM peak during the first 30 min in PBS remained negligible with a standard deviation of 5×10^{-6} in Δf/f (or 15 Hz in Δf), indicating the stability of the PEPS in liquid. The subsequent sulfo-SMCC bonding at 30–65 min, the HBVDM probe immobilization at 65–97 min indicated successful immobilization of the probe on the PEPS surface.

II.9. PEPS Regeneration

There were about 80 independent detection tests conducted in this study and only two PEPSs were used for all the detection tests. After each detection test, a PEPS was regenerated as follows before it was reused for another detection test. First, a PEPS was cleaned in a 1-in-100 diluted Piranha solution (two parts of 98% sulfuric acid (Fisher) with one part of 30% hydrogen peroxide (Fisher)) for 1 min followed by de-ionized (DI) water and ethanol rinsing. It was then soaked in a 0.1% MPS solution in ethanol with 0.5% DI water at pH 9 for MPS coating. The MPS solution was replaced with a fresh one every 12 h for 24 h or until the PEPS achieved a standard deviation of the WEM resonance frequency of < 20 Hz and a downshift of the WEM resonance frequency of < 20 Hz in PBS for 30 min.

II.10. Flow Setup and Spiked Urine Samples

The flow system for carrying out the detection contained a peristaltic pump (Cole-Parmer 77120–62) that drove the flow, a detection cell where detection took place, reservoirs containing DNA-spiked urine samples, FRMs, and PBS interconnected with tubing and valves as schematically shown in Fig. 2c. The flow cell was 18.5 mm long, 3.5 mm wide and 5.5 mm deep (volume = 356 μL). A schematic of the flow cell can be found in Kirimli et al.[44] The total internal volume of the flow cell plus tubing was approximately 1250 μL. The urine came from one individual. The subject was free of HBV infection or KRAS codon-12 mutations. The urine samples were collected in a “First Morning Specimen” manner, i.e., the bladder was emptied before bed and the sample was collected first thing in the morning. A total of 15 such urine samples were collected for the study and visually there was no significant difference among these 15 urine samples and 32 more that were used for previous studies.[36, 42, 44] In each detection experiment, the volume of the DNA-spiked urine sample was fixed at 10 ml and the probe-coated PEPS was placed in the center of the flow cell with the major faces of the PEPS parallel to the direction of the flow. The flow setup was placed inside an incubator (Digital Control Steel Door Incubator 10–180E, Quincy Lab) for temperature control. Because the top of the flow cell was open a 2-liter water bath was included in the incubator to minimize potential resonance frequency shift due to changes in the flow-cell liquid level by evaporation. The temperature of the urine sample reservoir was maintained at 95°C by means of a 95°C water bath on a hot plate. The urine sample was first loaded in the reservoir for 10 min to denature the DNA before turning on the pump. Once the pump was turned on, the 95°C-heated sample flowed from the reservoir through 1 m long ethyl vinyl acetate (EVA) tubing of a 0.8 mm inner diameter and a 2.4 mm outer

diameter (McMaster Carr) immersed in room-temperature water at a flow rate of 4 ml min^{-1} (corresponding to the fast-cooling scheme described in the supplemental information) to reach the detection cell where the PEPS was located for detection as schematically shown in Fig. 2c. How fast the denatured DNA could be cooled when it reached the detection cell was important in retaining the DNA in the denatured state[49] for the detection to occur in the detection cell. We examined three cooling schemes as detailed in the supplemental information. As was shown in the supplemental information, the fast-cooling scheme of passing the 95°C-treated urine sample through 1-m long tubing in a room-temperature water bath was the most effective among the three, retaining about 70% of the detection resonance frequency shift of single-stranded MT at the same concentration (see the supplemental). In what follows, all *in situ* double-stranded DNA detection tests were done using this cooling scheme. The temperature of the detection cell was 35°C for detecting HBVDM and 63°C for detection KRAS G12V.

For illustration purposes, following the probe immobilization shown in Fig. 2b, we ran the single-stranded HBVDM MT (ssMT) detection at 100 pM in PBS at 35°C and the subsequent FRMs detection at a 1×10^5 FRMs/ml in PBS at room temperature both at 2 mL min^{-1} using the flow system shown in Fig. 2c. The results were shown in Fig. 2b as the resonance frequency shift at 97–127 min and 127–157 min, respectively. Also shown in the inset in Fig. 2b is a schematic of the various steps involved in the immobilization process. Note the MT detection step shown in Fig. 2b was with single-stranded DNA (ssDNA) for illustration purposes.

II.11 Detection repeatability

For detection repeatability, for each detection condition and each DNA concentration, we repeated the detection three times. What we meant by that was that after each detection, we would regenerate the sensor. When the sensor was ready, we repeated the test. All the results shown below were the average of three independent tests for each detection condition and each concentration. As can be seen, the detection was quite repeatable.

III. RESULTS

III.1. Double-Stranded (ds) DNA detections in urine

For all dsDNA detection shown below, a flow system with the so-called fast-cooling scheme described above (see Fig. 2c) was used to *in situ* detect dsDNA in urine. In each test, 10 ml of urine spiked with a desired concentration dsDNA was loaded in the 95°C reservoir. A probe-coated PEPS was placed in the center of the detection cell to detect the target DNA in a flow of 4 ml/min for 30 min. Each detection was proceeded with 10 min of pre-heating in the reservoir to ensure all target double-stranded MT (dsMT) or double-stranded WT (dsWT) were fully de-hybridized when leaving the reservoir. To validate that the dsDNA detection, it was followed with *in situ* FRMs detection. Detections of ssDNA at the same concentrations were also carried out using the exactly the same flow conditions for comparison. Figures. 3a and Fig. 3b show the $-\Delta f/f$ versus time of dsMT detection followed by FRMs detection at various MT concentrations of HBVDM and KRAS, respectively. Also shown in Fig. 3a and Fig. 3b are $-\Delta f/f$ versus time of ssMT of HBVDM and KRAS at the

same concentrations followed the same FRMs detections. As can be seen, for both HBVDM and KRAS, the –Δf/f versus time of the dsMT detections are dose responsive and closely traced that of ssMT at the same concentration. Furthermore, the – Δf/f versus time of the FRMs detection following each dsMT detection was also MT dose responsive, similar to that of the FRMs detection following each ssMT detection. This, altogether indicates that the current flow system and cooling scheme were indeed capable of keeping the dsDNA de-hybridized and allow the targeted MT strand to be captured by the probe on the PEPS surface as illustrated in Fig. 3c which was evidenced by the subsequent FRMs detection by the captured targeted MT strands on the PEPS surface as illustrated in Fig. 3d.

To more closely examine the efficacy of the current dsMT and dsWT detection methodology as against ssMT and ssWT detection, in Fig. 4a and Fig. 4b, we plot $(-\Delta f/f)_{ave}$ versus concentration for dsMT (open squares), dsWT (open circles), ssMT (full squares), and ssWT (full circles) for HBVDM and KRAS, respectively where $(-\Delta f/f)_{ave}$ represents the average detection –Δf/f over the last five minutes (t = 25–30 min) of the detection. Note the $(-\Delta f/f)_{ave}$ of dsMT at each concentration was close to that of ssMT at the same concentration and the $(-\Delta f/f)_{ave}$ of dsWT at each concentration was also close to that of ssWT at the same concentration for both HBVDM and KRAS. Furthermore, the $(-\Delta f/f)_{ave}$ of WT was much smaller than that of MT whether double-stranded (ds) or single-stranded, indicating that the current dsMT detection (1) exhibited similarly high efficacy as ssMT detection and (2) also similarly high specificity against WT detection as ssMT. To quantify the effectiveness of dsMT detection against ssMT we plot the ratio $(-\Delta f/f)_{ave,dsMT}/(-\Delta f/f)_{ave,ssMT}$ versus MT concentration in Fig. 4c where $(-\Delta f/f)_{ave,dsMT}$ was the $(-\Delta f/f)_{ave}$ of dsMT and $(-\Delta f/f)_{ave,ssMT}$ was the $(-\Delta f/f)_{ave}$ of ssMT at the same MT concentration. As can be see, all ratios ranged 0.7 or higher, confirming that the current fast cooling method was effective in keeping DNA de-hybridized, as consistent with initial data for the fast cooling method shown in the supplemental information. Note the same methodology was also effective in detecting dsWT against ssWT. Due to the weaker binding of WT with the probe, both (–Δf/f)ave,dsWT and (–Δf/f)ave,ssWT, and hence (–Δf/f)ave,dsWT/(–Δf/f)ave,ssWT was only meaningful at concentrations 10^{-14} M or higher. For this reason the $(-\Delta f/f)_{ave,dsWT}/(-\Delta f/f)_{ave,ssWT}$ versus concentration plot is included in the supplemental information. To examine if dsMT detection was specific enough against a high background (BG) of WT such as 250-fold WT for HBVDM and 1000-fold WT for KRAS, we plot the ratio $(-\Delta f/f)_{ave,BG}/(-\Delta f/f)_{ave,MT}$ versus MT concentration in Fig. 4d where the subscript, BG, stands for WT at a concentration 250-fold that of MT for HBVDM and 1000-fold that of MT for KRAS. As can be seen, even with 250-fold more WT (for HBVDM) or 1000-fold more WT (for KRAS), $(-\Delta f/f)_{ave,BG}/(-\Delta f/f)_{ave,MT}$ was still less than 0.2 for dsMT and ssMT concentrations 10^{-18} M or higher and <0.36 for dsMT and ssMT concentrations at 10^{-19} M, indicative that even at such a high background of WT, the main contribution of the -Δf/f came from dsMT detection (as similar to ssMT) but not the WT background. To better illustrate this, we further plot estimated fraction of the MT signal defined as $(-\Delta f/f)_{ave,MT}/[(-\Delta f/f)_{ave,BG}+(-\Delta f/f)_{ave,MT}]$ versus MT concentration as the insert in Fig. 4d. Clearly, for both dsMT and ssMT, all fractions of MT signals were larger than 0.8, indicating that most of the detection signal was from dsMT even in such a high background of WT as similar to the results of the ssMT detections.

III.2. dsMT detection in urine in a background of dsWT

dsMT detections at various dsMT concentrations were carried out in urine samples containing a background (BG) of dsWT−−250-fold for HBVDM and 1000-fold for KRAS. -Δf/f versus time of such detections are shown in Fig. 5a for HBVDM and Fig. 5b for KRAS. The resultant $(-\Delta f/f)_{ave,dsMT}/(-\Delta f/f)_{ave,ssMT}$ for HBVDM in 250-fold WT and that for KRAS in 1000-fold WT are also included in Fig. 4c. As can be seen, the dsMT detection remained more or less the same even with the high background (BG) of WT. The dsMT detections shown in Figs. 5a and 5b were followed with FRMs detections between t=30 min and t=60 min. The fluorescence micrographs of the PEPS surface after FRMs detections are shown in Figs. 5c-5f for HBVDM and in Figs. 5g-5j for KRAS. Note that the number of captured FRMs increased with an increasing MT concentration for both HBVDM and KRAS. These fluorescent micrographs validated the dsMT detection results shown in Figs 5a and 5b as without the target MT being captured on the PEPS surface during the dsMT detection it would not have been possible for the PEPS the FRMs during the subsequent FRMs detection.

III.3. KRAS detection from SW480 DNA in urine.

Detection of KRAS mutation was carried out at various concentration of SW480 DNA fragments spiked in urine. The resultant -Δf/f versus time of KRAS mutation detection at various SW480 DNA fragments concentrations followed with FRMs detection is shown in Fig. 6a. Fluorescence micrographs of the captured FRMs after the FRMs detections are shown in Figs. 6b-6e. To compare the detection results of the SW480 NA fragment with that of the synthetic KRAS dsMT detection results shown in Fig. 4b the obtained $(-\Delta f/f)_{ave}$ of the SW480 NA fragment detections are also plotted in Fig. 4b. As can be seen, the $(-\Delta f/f)_{ave}$ overlapped with those of synthetic dsMT within the error bars at the same MT concentrations, and the FRMs micrographs shown in Figs 6b-6e were also similar to those shown in Figs. 5g-5j of the same MT concentrations. This indicates that the same dsMT detection methodology was equally effective in detecting KRAS mutation from naturally occurring DNA fragments derived from SA480 cells as from the synthetic dsMT and confirms that the current methodology could indeed be applied to detect double-stranded MT derived from cell lines.

IV. DISCUSSIONS

There were two reasons for the current cooling scheme to be so effective in keeping the DNA dehybridized. The first was that the rapid heat transfer across the tubing wall was made possible by the long and narrow tubing geometry. This can be seen as follows. With the flow rate being 4 ml/min and an inner tubing diameter being 0.8 mm the average flow speed of the stool, v, was 0.13 m/s and the time it took to travel the 1 m long tubing was only 7.5 s. This was the time allowed to cool the stool from the reservoir temperature to the detection temperature. Given the tubing geometry, the heat absorbed per second by the water bath through thermal conduction across the tubing wall could be estimated as[50] $Q_c = 2kl(T_s - T_w)/\ln(r_o/r_i)$ where k was the thermal conductivity of the EVA tubing, l was the length of the tubing, r_o and r_i were respectively the outer and inner diameters of the tubing, T_s the average temperature of the stool inside the tubing, and T_w the temperature of the water bath. Given k

= 0.23 J/(s.m.K)[51], T_w = 20°C, r_o = 1.2 mm and r_i = 0.4 mm, and T_s were taken to be 65°C for HBVDM detection and 79°C for KRAS detection, we estimated Q_c = 19 J/s and 25 J/s for HBVDM detection and KRAS detection, respectively. On the other hand, the heat that must have been removed from the stool per second to allow the temperature of the stool to drop from the reservoir temperature, T_r, to the detection cell temperature, T_d when arriving at the detection could be estimated as $Q_r = c_p \rho(\pi r_i^2) v(T_r - T_d)$ where c_p and ρ were the specific heat and density of the stool, r_i the inner radius of the tubing, v the average flow speed of the stool. With c_p = 4186 J/(kg.K),[52] ρ=1000 kg/m^3, r_i =0.4 mm, T_r =95°C, and T_d =35°C for HBVDM detection and 63°C for KRAS detection, we estimated Q_r = 16 J/s and 8.7 J/s for HBVDM detection and KRAS detection, respectively. As can be seen, Q_c was larger than Q_r for both HBVDM and KRAS detections. This indicates that the current setup was indeed capable of removing enough heat to cool the stool sample fast enough so that when the stool reached the detection cell its temperature has also dropped to the detection temperature. The second reason was that the DNA molecules were carried by a steady laminar flow, which can be seen as follows. Given d_i = 0.8 mm was the tube inner diameter, v = 0.13 m/s the average flow velocity, η = 1 mPa.s the viscosity of the fluid, and ρ = 1000 kg/m^3, the density of the fluid, the Reynolds number,[53] Re = ρ v d_i / η for the flow in the narrow tubing was only 100, which was well within the boundary of 2300 for a laminar flow.[53] It is known that fluid flows in a laminar flow stays in its own layer without lateral mixing. Thus the DNA molecules were mostly traveling within a layer of the fluid flow without much transverse movement, thus greatly limiting the chances for DNA molecules to re-hybridize. Further considering the low DNA concentrations, for instance, 10^{-19} M (60 copies/ml), there would only be about 30 copies of each strand in the entire 1-m length of the tubing--or one DNA copy per 3 cm of tubing. It was highly unlikely that any of these DNA molecules would collide with one another and re-hybridize within the tubing. Even at a higher concentration, for example, 10^{-16} M (60,000 copies/ml), there would still only be 30 copies of DNA per mm length, still quite sparse considering the size of the DNA molecules, each DNA molecule would still be traveling in its own layer of the laminar flow without colliding with another DNA molecule, thus effectively preventing DNA molecules from re-hybridizing before reaching the detection cell.

V. CONCLUSIONS

We have investigated *in situ* amplification-free double-stranded mutation detection in urine using piezoelectric plate sensors (PEPs) in a close-loop flow with two temperature zones. The high-temperature zone dubbed the reservoir maintained at 95°C was where the sample was loaded and DNA de-hybridized. The heated urine was cooled by flowing at a flow rate of 4 ml/min through a 1 m long tubing with an inner diameter of 0.8 mm immersed in a room-temperature water bath to reach the detection cell kept at the desire detection temperature where the detection took place. Using HBVDM and KRAS G12V as model mutations, it was shown that with such a cooling scheme in a flow PEPS was able to detect double-stranded mutations with 70% detection efficiency or better at concentrations ranging 10^{-19}M – 10^{-16}M against single-stranded DNA detection at the same concentrations as validated by *in situ* detection of fluorescent reporter microspheres (FRMs) following the double stranded mutation detections as well as microscopic visualization of FRMs following

the FRMs detection. We have also demonstrated such double-stranded mutation detection was still effective at 10^{-19} M – 10^{-16} M while in a background of 250-fold wildtype for HBVDM and 1000-fold wildtype for KRAS. Also demonstrated was detection of KRAS mutation at 10^{-19}M – 10^{-16}M SW480 DNA fragments in urine. Furthermore, it has been demonstrated that there were no interferences between sensors when multiple sensors were used in multiplexed detection tests[43, 54] Therefore, the highly specific *in situ*, amplification-free and label-free mutation detection can be conducted in a multiplexed fashion.

Supplementary Material

Refer to Web version on PubMed Central for supplementary material.

ACKNOWLEDGMENT

This work was supported in part by the National Institute of Health Grants No. 1R41AI1122224 and 1R41AI120445 and Pennsylvania Department of Health.

REFERENCES:

1. Crowley E, Di Nicolantonio F, Loupakis F and Bardelli A, Nat Rev Clin Oncol, 2013, 10, 472–484. [PubMed: 23836314]
2. Robertson EG and Baxter G, Clinical radiology, 2011, 66, 1007–1014. [PubMed: 21784421]
3. Lipsky RH, Mazzanti CM, Rudolph JG, Xu K, Vyas G, Bozak D, Radel MQ and Goldman D, Clin Chem, 2001, 47, 635–644. [PubMed: 11274012]
4. Caruso F, Rodda E, Furlong DN, Niikura K and Okahata Y, Analytical Chemistry, 1997, 69, 2043–2049. [PubMed: 21639244]
5. Su YH, Wang M, Block TM, Landt O, Botezatu I, Serdyuk O, Lichtenstein A, Melkonyan H, Tomei LD and Umansky S, Ann N Y Acad Sci, 2004, 1022, 81–89. [PubMed: 15251944]
6. Su YH, Wang MJ, Brenner DE, Ng A, Melkonyan H, Umansky S, Syngal S and Block TM, Journal of Molecular Diagnostics, 2004, 6, 101–107. [PubMed: 15096565]
7. Umansky SR and Tomei LD, Expert Rev Mol Diagn, 2006, 6, 153–163. [PubMed: 16512776]
8. Hammond DM, Manetto A, Gierlich J, Azov VA, Gramlich PM, Burley GA, Maul M and Carell T, Angew Chem Int Ed Engl, 2007, 46, 4184–4187. [PubMed: 17458844]
9. Passamano M and Pighini M, Sensors and Actuators B: Chemical, 2006, 118, 177–181.
10. Feng K, Li J, Jiang JH, Shen GL and Yu RQ, Biosens Bioelectron, 2007, 22, 1651–1657. [PubMed: 16963256]
11. Gasparac R, Taft BJ, Lapierre-Devlin MA, Lazareck AD, Xu JM and Kelley SO, Journal of the American Chemical Society, 2004, 126, 12270–12271. [PubMed: 15453752]
12. Park SJ, Taton TA and Mirkin CA, Science, 2002, 295, 1503–1506. [PubMed: 11859188]
13. He L, Musick MD, Nicewarner SR, Salinas FG, Benkovic SJ, Natan MJ and Keating CD, Journal of the American Chemical Society, 2000, 122, 9071–9077.
14. Mao X, Yang L, Su XL and Li Y, Biosens Bioelectron, 2006, 21, 1178–1185. [PubMed: 15951163]
15. Gifford LK, Sendroiu IE, Corn RM and Luptak A, J Am Chem Soc, 2010, 132, 9265–9267. [PubMed: 20565098]
16. Yang T, Zhou N, Zhang Y, Zhang W, Jiao K and Li G, Biosens Bioelectron, 2009, 24, 2165–2170. [PubMed: 19131238]
17. Zheng G, Patolsky F, Cui Y, Wang WU and Lieber CM, Nat Biotechnol, 2005, 23, 1294–1301. [PubMed: 16170313]
18. Zhang GJ, Luo ZH, Huang MJ, Tay GK and Lim EJ, Biosens Bioelectron, 2010, 25, 2447–2453. [PubMed: 20435462]

19. Andreu A, Merkert JW, Lecaros LA, Broglin BL, Brazell JT and El-Kouedi M, Sensors and Actuators B: Chemical, 2006, 114, 1116–1120.
20. Gao Z, Agarwal A, Trigg AD, Singh N, Fang C, Tung CH, Fan Y, Buddharaju KD and Kong J, Anal Chem, 2007, 79, 3291–3297. [PubMed: 17407259]
21. Hahm J.-i. and Lieber CM, Nano Letters, 2003, 4, 51–54.
22. Wang J, Polsky R, Merkoci A and Turner KL, Langmuir, 2003, 19, 989–991.
23. Chang H, Yuan Y, Shi N and Guan Y, Anal Chem, 2007, 79, 5111–5115. [PubMed: 17530821]
24. Su M, Li S and Dravid VP, Applied Physics Letters, 2003, 82, 3562–3564.
25. Rijal K and Mutharasan R, Anal Chem, 2007, 79, 7392–7400. [PubMed: 17764156]
26. Zheng S, Choi JH, Lee SM, Hwang KS, Kim SK and Kim TS, Lab on a Chip, 2011, 11, 63–69. [PubMed: 21060947]
27. Wang J, Kawde AN and Musameh M, Analyst, 2003, 128, 912–916. [PubMed: 12894830]
28. Husale S, Persson HH and Sahin O, Nature, 2009, 462, 1075–1078. [PubMed: 20010806]
29. Kurkina T, Vlandas A, Ahmad A, Kern K and Balasubramanian K, Angew Chem Int Ed Engl, 2011, 50, 3710–3714. [PubMed: 21425218]
30. Chen C-P, Ganguly A, Lu C-Y, Chen T-Y, Kuo C-C, Chen R-S, Tu W-H, Fischer WB, Chen K-H and Chen L-C, Anal Chem, 2011, 83, 1938–1943. [PubMed: 21351780]
31. Gao W, Dong H, Lei J, Ji H and Ju H, Chem Commun (Camb), 2011, 47, 5220–5222. [PubMed: 21461429]
32. Soleymani L, Fang Z, Kelley SO and Sargent EH, Applied Physics Letters, 2009, 95, 143701–143703.
33. Loaiza OA, Campuzano S, Pedrero M, Pividori MI, Garcia P and Pingarron JM, Anal Chem, 2008, 80, 8239–8245. [PubMed: 18837513]
34. Shih WY, Luo H, Li H, Martorano C and Shih W-H, Applied Physics Letters, 2006, 89, 242913–242913.
35. Wu W, Kirimli CE, Shih WH and Shih WY, Biosens Bioelectron, 2013, 43, 391–399. [PubMed: 23356996]
36. Kirimli CE, Shih WH and Shih WY, Analyst, 2014, 139, 2754–2763. [PubMed: 24759937]
37. Zhu Q, Shih WY and Shi WH, Sensors and Actuators B-Chemical, 2009, 138, 1–4.
38. Zhu Q, Shih WY and Shih W-H, Applied Physics Letters, 2008, 92, 183505. [PubMed: 19479043]
39. Shih WY, Zhu Q and Shih WH, Journal of Applied Physics, 2008, 104.
40. Zhu Q, Shih WH and Shih WY, Sensors and Actuators B-Chemical, 2013, 182, 9.
41. Wu W, Shih WY and Shih WH, Journal of Applied Physics, 2013, 114.
42. Kirimli CE, Shih WH and Shih WY, Analyst, 2015, 140, 1590–1598. [PubMed: 25599103]
43. Kirimli CE, Shih WH and Shih WY, Analyst, 2016, DOI: 10.1039/c5an02048d.
44. Kirimli CE, Shih WH and Shih WY, Analyst, 2016, 141, 1421–1433. [PubMed: 26783561]
45. Kirimli CE, Shih WH and Shih WY, Analyst, 2013, 138, 6117–6126. [PubMed: 23964355]
46. Kirimli CE, Shih WH and Shih WY, Methods in molecular biology (Clifton, N.J.), 2017, 1572, 327–348.
47. Soylu MC, Shih W-H and Shih WY, Industrial & Engineering Chemistry Research, 2013, 52, 2590–2597.
48. Soylu MÇ, Drexel University, 2013.
49. Doty P, Marmur J, Eigner J and Schildkraut C, Proceedings of the National Academy of Sciences of the United States of America, 1960, 46, 461–476. [PubMed: 16590628]
50. Theodore L, Heat Transfer Applications for the Practicing Engineer, Wiley, Hoboken, New Jersey, 2011.
51. Allan J, Pinder H and Dehouche Z, AIP Advances 2016, 6, 9.
52. Sears FW, Zemansky MW and Young HD, University Physics, Addison-Wiley, United States, 1980.
53. Truskey GA, Y. F. and Katz DF, Transport Phenomena in Biological Systems, Pearson Rrentice Hall, Upper Saddle Revier, New Jersey, 2nd edn.

54. McGovern JP, Shih WH, Rest RF, Purohit M, Mattiucci M, Pourrezaei K, Onaral B and Shih WY, Review of Scientific Instruments, 2009, 80.

Highlights

- Piezoelectric sensor contains a flow system that de-hybridizes double-stranded DNA
- Double-stranded mutations are detected in situ without isolation or amplification
- The detection was in urine without label with 60 copies/ml sensitivity
- KRAS and hepatitis B virus double mutation detected in 1000-fold wildtype background
- Double-stranded detection was 80 percent as effective as single-stranded detection.

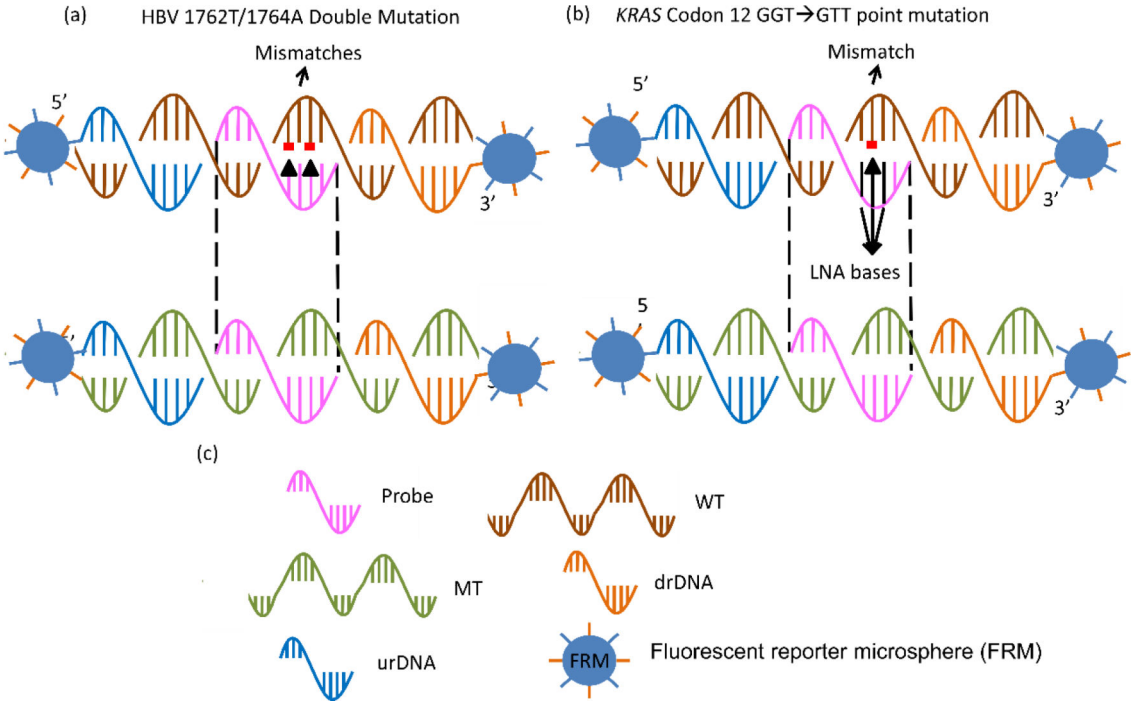

Figure 1:

(a) A schematic of the relationship between probe, mutant (MT) target DNA (tDNA), wild type (WT), downstream reporter DNA (drDNA), and upstream reporter DNA (urDNA) for HBV 1762/1764 double mutation, (b) that for *KRAS* point mutation, and (c) the legend defining probe, MT, WT, drDNA, urDNA and fluorescent reporter microsphere (FRM) that was evenly coated with urDNA and drDNA.

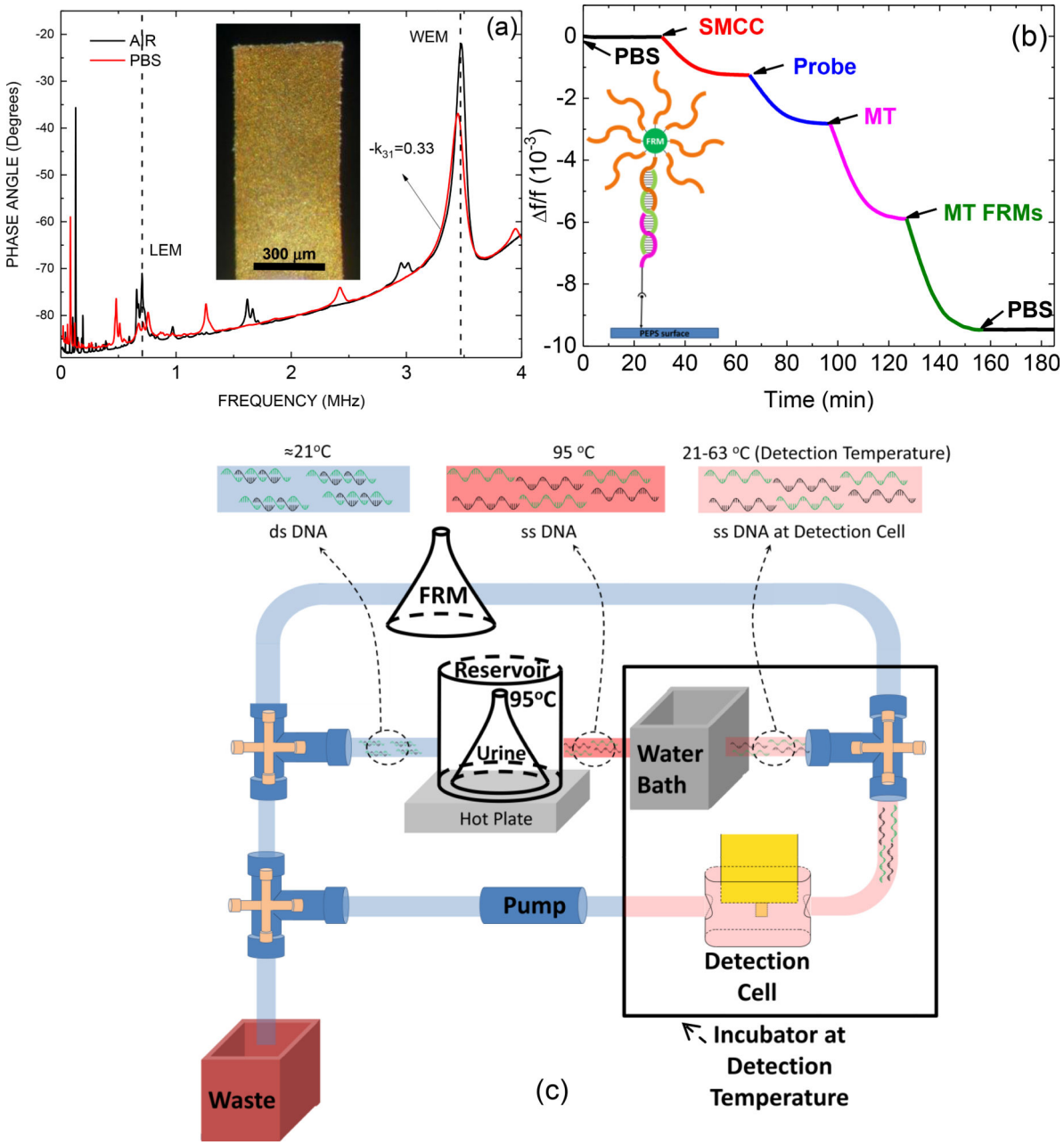

Figure 2.

(a) In-air (black) and in-PBS (red) phase angle-versus-frequency resonance spectra with an insert showing an optical micrograph of the PEPS, (b)) relative resonance frequency shift, Δf/f, of the PMN-PT PEPS going through PBS step (0–30 min), the SMCC bonding step (30–65 min), the probe immobilization step(65–97 min), the MT detection step (97–127 min), the MT FRMs detection step (127–157 min), and the final PBS step (157–180 min) with an insert showing a schematic of the molecules involved in these steps, and (c) a schematic of flow system for *in situ* de-hybridization and detection of double-stranded DNA. Note the MT detection at 97–127 min in (b) involved only single-stranded MT for illustration of the various binding steps and did not involve the flow system shown in (c).

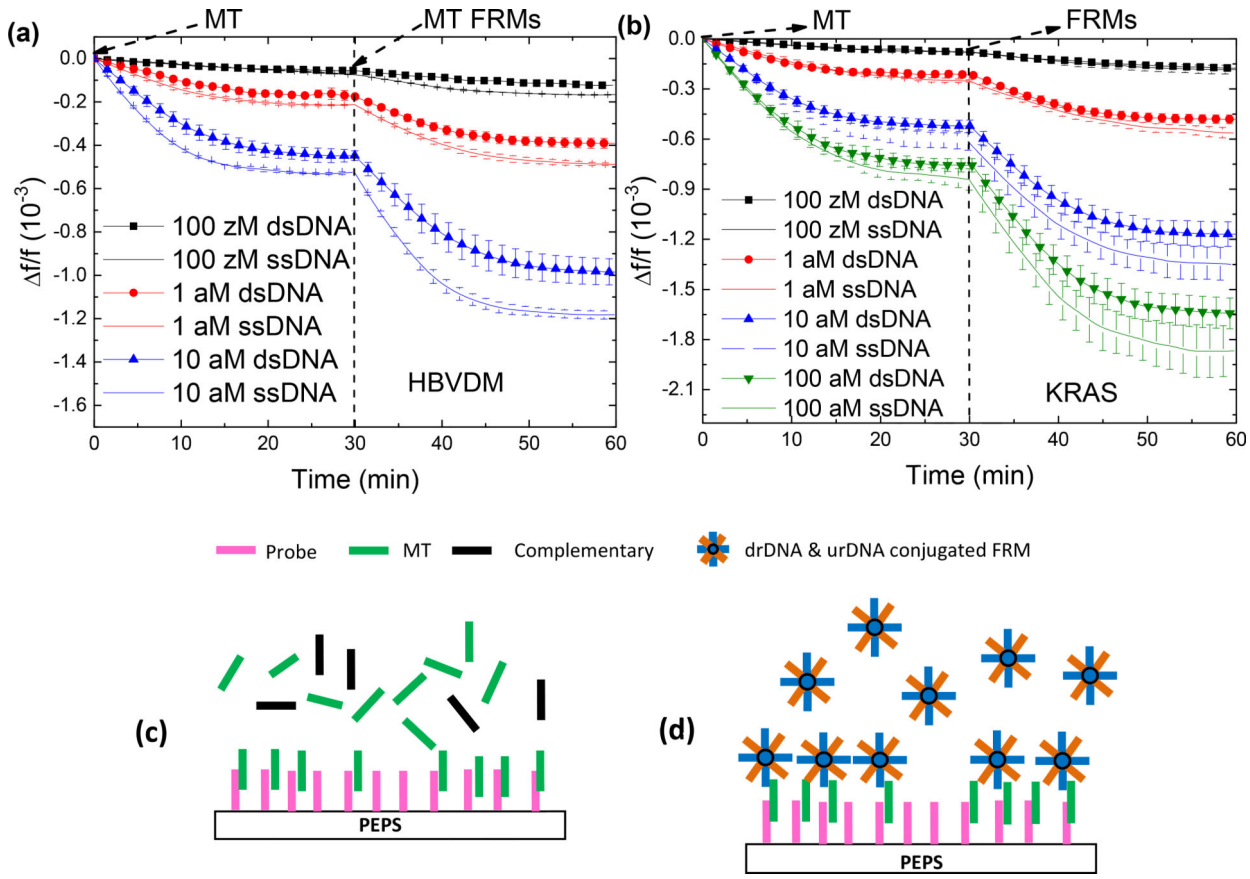

Figure 3.

Δf/f versus time of dsMT detection and the following FRMs detection at various concentrations of MT for (a) HBVDM and (b) KRAS. Also shown in (a) and (b) are the results of ssMT detections at the same concentrations as for comparison. (c) A schematic representation of dsMT detection, and (d) that of FRMs detection following the MT detection.

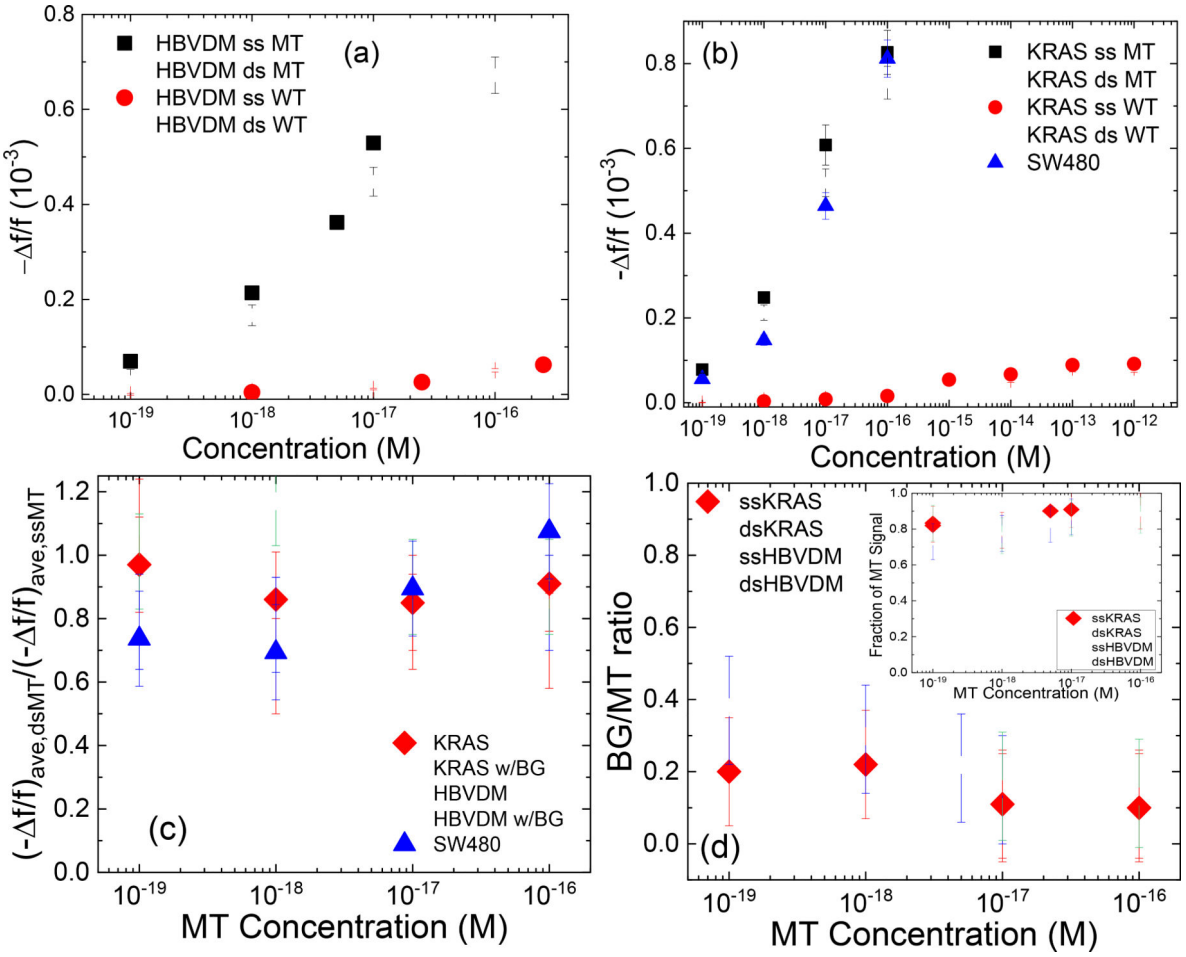

Figure. 4:

$(-\Delta f/f)_{ave}$ of dsMT detection (open squares), ssMT detection (full squares), dsWT detection (open circles), and ssWT detection (full circles) at various concentrations for (a) HBVDM and (b) KRAS; (c) $(-\Delta f/f)_{ave,dsMT}/(-\Delta f/f)_{ave,ssMT}$ versus MT concentration with full diamonds for KRAS and open triangles for HBVDM; (d) $(-\Delta f/f)_{ave,BG}/(-\Delta f/f)_{ave,MT}$ versus MT concentration where "BG" in the subscript denotes dsWT detection at a "BG" concentration, which was 250-fold that of MT for HBVDM and 1000-fold that of MT for KRAS, respectively. The insert in (d) shows estimated fraction of MT signal versus MT concentration where the estimated fraction of MT signal is defined as $(-\Delta f/f)_{ave,MT}/[(-\Delta f/f)_{ave,MT}+(-\Delta f/f)_{ave,BG}]$ with $(\Delta f/f)_{ave,BG}$ being the $(-\Delta f/f)_{ave}$ of WT at the BG concentration and $(-\Delta f/f)_{ave}$ being the average - Δf/f of t = 25–30 min. Also shown in (c) are the detection results ds HBVDM with 250-fold WT (open down triangles) and ds KRAS with 1000-fold WT (open circles) as well as that of DNA fragments from SW480 cells (full up triangles).

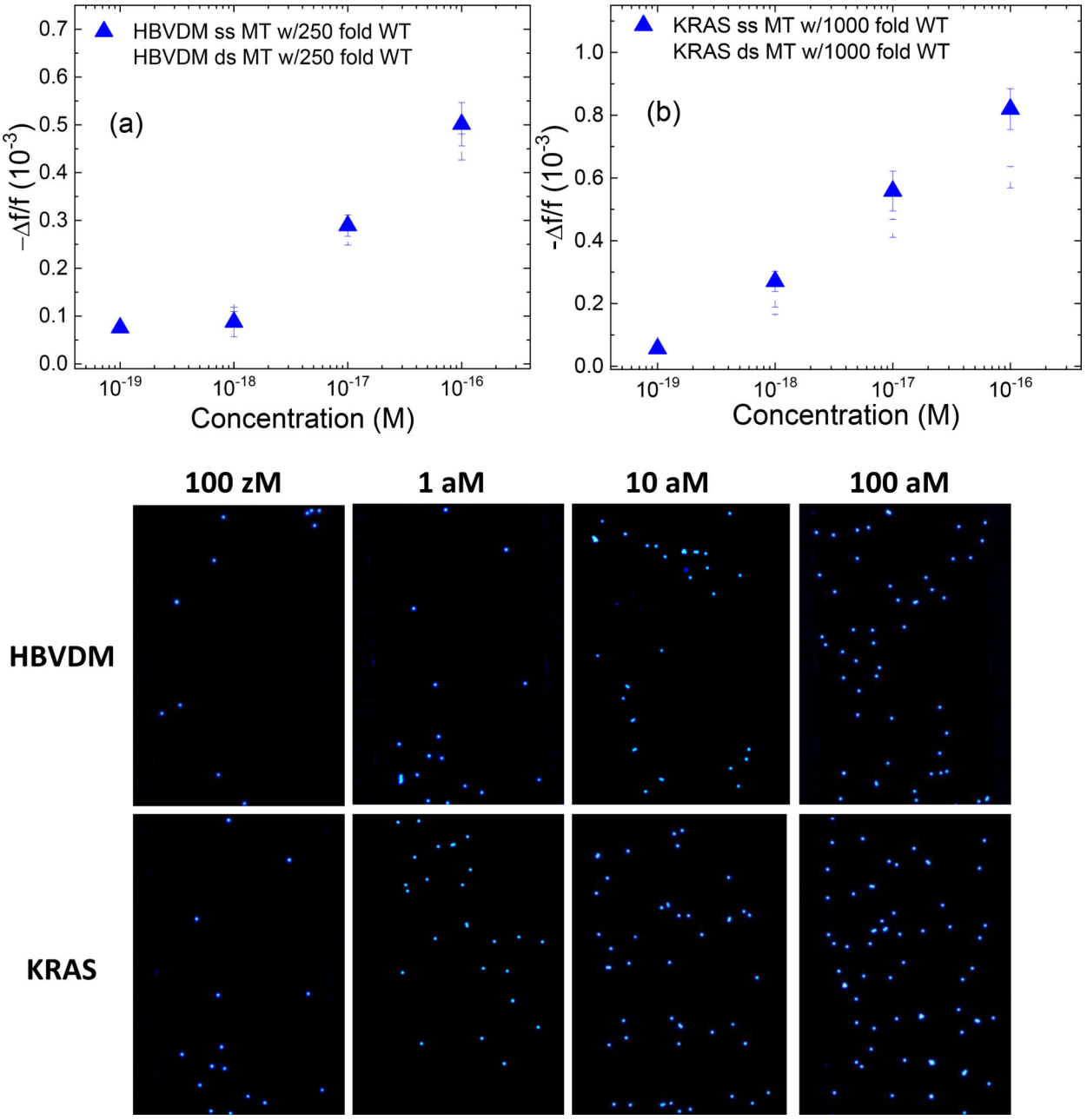

Figure 5:

Average -Δf/f at 25–30 minutes versus concentration of dsMT detection for (a) HBVDM in a background of 250-fold dsWT and that for (b) *KRAS* in a background of 1000-fold dsWT, which was followed by detection in a mixture of 10^5 FRMs/ml of FRMs in PBS. (c), (d), (e), and (f) are the fluorescent images of the PEPS obtained after the FRMs detection following the HBVDM MT detections at 0.1 aM (100 zM), 1 aM, 10 aM, and 100 aM MT concentrations, respectively and (g), (h), (i) and (j) are the fluorescent images of the PEPS obtained after the FRMS detection following the *KRAS* MT detections at 0.1 aM (100 zM), 1 aM, 10 aM, and 100 aM MT concentrations, respectively.

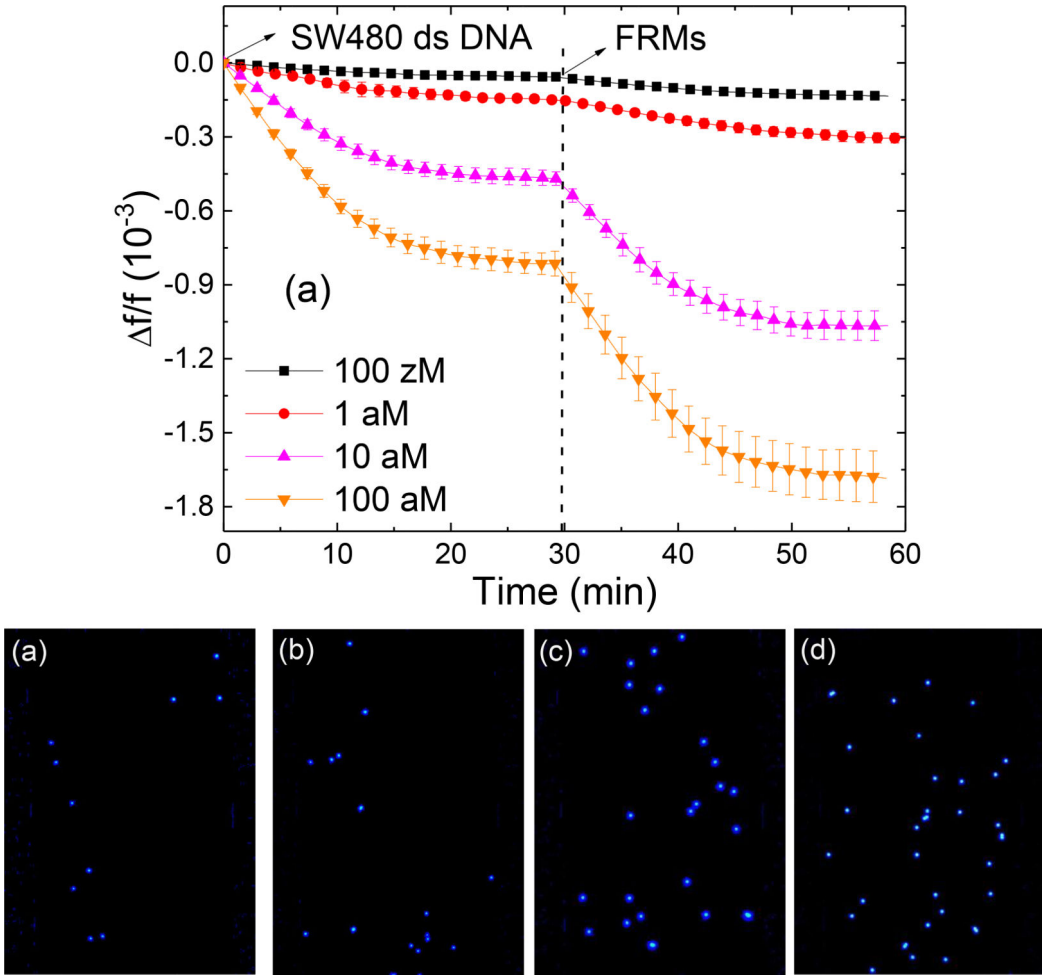

Figure 6:

(a) -Δf/f versus time of PEPS detection of SW480 DNA fragments followed by detection in a mixture of 10^5 FRMs/ml of FRMs in PBS, (b), (c), (d) and (e) are the fluorescent images of the PEPS obtained after the FRMS detection following the SW480 DNA fragment detections at 0.1 aM (100 zM), 1 aM, 10 aM, and 100 aM concentrations, respectively.